Lagrangian evolution of velocity increments in rotating turbulence: the effects of rotation on non-Gaussian statistics

Yi Li

School of Mathematics and Statistics, The University of Sheffield, Sheffield, South Yorkshire, S3 7RH, UK

Abstract

The effects of rotation on the evolution of non-Gaussian statistics of velocity increments in rotating turbulence are studied in this paper. Following the Lagrangian evolution of the velocity increments over a fixed distance on an evolving material element, we derive a set of equations for the increments, which provides closed representation for the nonlinear interaction between the increments and the Coriolis force. Applying a restricted-Euler-type closure to the system, we obtain a system of ordinary differential equations, which retains the effects of nonlinear interaction between the velocity increments and the Coriolis force. *A-priori* tests using direct numerical simulation data show that the system captures important dynamics of rotating turbulence. The system is integrated numerically starting from Gaussian initial data. It is shown that the system reproduces qualitatively a number of observations in rotating turbulence. The statistics of the velocity increments tend to Gaussian when strong rotation is imposed. The negative skewness in the longitudinal velocity increments is weakened by rotation. The model also predicts that the transverse velocity increment in the plane perpendicular to the rotation axis will have positive skewness, and that the skewness will depend on the Rossby number in a non-monotonic way. Based on the system, we identify the dynamical mechanisms leading to the observations.

Keywords: Fluid dynamics, Geophysical flows, Turbulence, Rotating frame, Intermittency

1. Introduction

Rotating turbulence plays an important role in many different areas, including geophysical, astrophysical and engineering applications. In rotating turbulence, the effects of rotation enter through the Coriolis force [1, 2]. The

Email address: yili@sheffield.ac.uk (Yi Li)

relative importance of the Coriolis force in homogeneous turbulence is qualitatively measured by the Rossby number defined as the ratio of the nonlinear advection term to the Coriolis force. There has been a continuous effort to understand the effects of the Coriolis force that have led to the peculiar features of rotating turbulence. It is known that in rotating turbulence the energy transfer in the Fourier space is weakened by the phase-scrambling effects generated by the inertial waves [3, 4]. As a consequence, steeper energy spectrum is observed in simulations and experiments [5, 6, 7, 8, 9], which is also predicted by phenomenological and analytical models [10, 11]. On the other hand, it is argued that the nonlinear interaction between resonant waves is largely responsible for the generation of coherent columnar vortex structures, the tendency towards two-dimensionalization, inverse energy cascade, and a number of other phenomena [12, 13, 6, 14, 8, 15], although recently it is shown that linear mechanisms may also make important contributions [16, 17].

For non-rotating turbulence, the small-scale structures of turbulence have received considerable attention. Measured by velocity increments and velocity gradients, the statistics at small scales have been shown to be highly non-Gaussian (see, e.g., [18]). The non-Gaussian statistics are generated by frequent, intense fluctuations in small scale quantities, which presents great obstacles to the efforts to develop universal models. Similar approaches have been adopted in the study of the small-scale structure of rotating turbulence recently. The statistics of velocity gradients have been studied in [19]. It is observed that, generally, the statistics tend to become more Gaussian in rotating turbulence. A phenomenon that has received considerable attention is the observation that the vertical vorticity component displays positive skewness, which takes the maximum at some intermediate value of the Rossby number[13, 15, 20]. Visually, the observation is related to the prevalence of cyclonic vortices in rotating turbulent fields. It is observed that the maximum in the skewness coincides with the maximum in the three-dimensional to two-dimensional energy transfer [15]. The phenomenon has been attributed to the instability of anti-cyclonic vortices in [13]. On the other hand, [21] shows that the initial growth of the skewness is proportional to the product between the rotation rate of the frame of reference and the mean vortex stretching. Since the mean vortex stretching is positive in an isotropic turbulence, this will lead to an algebraic growth in the skewness when rotation is imposed. Using data generated by direct numerical simulations (DNS), [20] studies the problem in great detail and concludes that the stationary value of the skewness are affected by a number of other parameters. The properties of velocity increments have also been documented in the experimental and/or DNS studies reported in [22, 19, 9, 23, 24, 25]. The scaling law of the velocity increments is measured, showing reduced anomalous scaling. Skewness of the longitudinal velocity increments is also observed to be weakened by rotation. Several phenomenological models are proposed to explain the observations regarding the scaling law in rotating turbulence [22, 25].

Thus, it appears that there is not yet consensus as to the mechanisms of some observations regarding the non-Gaussian statistics in velocity increments and velocity gradients. In particular, the understanding based on the dynamics

of the governing Navier-Stokes (NS) equations is desirable. In this paper, we intend to provide a partial yet unified explanation for a number of observations via a simple dynamical model. To provide the background for the model, we note that it is closely related to recent research on the so-called restricted Euler approximation and several models for the small-scale dynamics of turbulence. In the restricted Euler (RE) approximation, the equation for the velocity gradient is truncated, and only the nonlinear term and the isotropic part of the pressure Hessian are retained [26, 27]. The velocity gradient predicted from the RE approximation develops a finite time singularity. However the tensorial structure of the gradient reproduces a number of important features observed in turbulence, such as the preferential alignment between the vorticity vector and the intermediate eigen-direction of the strain rate tensor [26, 27, 28, 29]. Thus, the RE approximation has been used as a base model to understand the small-scale turbulence. A number of models for the pressure Hessian have been proposed to regularize the approximation. A useful idea is to follow the Lagrangian evolution of material elements, which has been pursued in [30, 31, 32, 33] (see also [34] for a recent model). The ideas are adopted to study the evolution of veloicty increments in [35]. A simple dynamical model for the velocity increments is derived by following the Lagrangian evolution of a linear element [35]. The model is generalized to turbulence in two and four spatial dimensions, and to include the increments of passive scalars in [36]. These models reproduce quite a few important observations regarding the non-Gaussian statistics of the increments, thus have helped clarify the origins of the observations from a dynamical point of view. It is also predicted that the increments of a passive scalar [36] are more intermittent in four spatial dimensions (compared with three spatial dimensions). In this paper, we applied the ideas to study the evolution of the non-Gaussian statistics of velocity increments in rotating turbulence. In order to incorporate the Coriolis force, a local coordinate system attached to an evolving material line is introduced. We show that, with the help of the coordinate system, a system of equations for the velocity increments over a fixed distant on the material line can be derived. The analysis of a restricted-Euler-type approximation of the system shows that several features of rotating turbulence can be reproduced, which thus provides explanations to some of the observations from a dynamical perspective.

The paper is organized as follows: In section 2, the system of the equations is derived, and an *a-priori* analysis is conducted. The numerical solution of the system is presented in the section 3. Conclusions are summarized in section 4.

2. Derivation of the equations and a-priori tests

Following the idea of [35, 36], we keep track of a line element $\mathbf{r}(t)$ and consider the velocity increments over a fixed distance ℓ along the direction of the element $\hat{\mathbf{r}}(t) \equiv \mathbf{r}/r$, where $r \equiv |\mathbf{r}|$ is the length of the line element. In [35, 36], where non-rotating turbulence is considered, a system of two equations for the longitudinal and transverse velocity increments over ℓ is derived. In rotating turbulence, however, we first need to define a local Cartesian coordinate system in order to

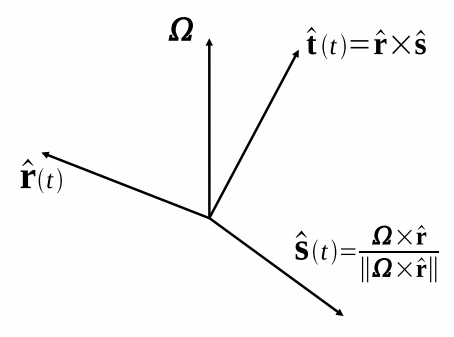

Figure 1: The local coordinate frame defined by the direction of a line element $\hat{\mathbf{r}}$ and rotation direction.

better account for the effects of the Coriolis force. Suppose the rotation axis is $\mathbf{k}$, so that the angular velocity of the frame of reference is $\boldsymbol{\Omega} = \Omega\mathbf{k}$, which is independent of time. We define the local Cartesian coordinate system by the following three unit vectors (see Fig. 1):

$$\hat{\mathbf{r}}(t),\ \hat{\mathbf{s}}(t) = \boldsymbol{\Omega} \times \hat{\mathbf{r}}/||\boldsymbol{\Omega} \times \hat{\mathbf{r}}||,\ \hat{\mathbf{t}}(t) = \hat{\mathbf{r}} \times \hat{\mathbf{s}}. \tag{1}$$

With $\mathbf{u}(\mathbf{x}, t)$ denoting the velocity field, in the above local coordinate frame the velocity increment can be decomposed into three components:

$$\delta\mathbf{u} \equiv \mathbf{u}(\mathbf{x} + \ell\hat{\mathbf{r}}, t) - \mathbf{u}(\mathbf{x}, t) = U\hat{\mathbf{r}} + V\hat{\mathbf{s}} + W\hat{\mathbf{t}}. \tag{2}$$

That is, U denotes the longitudinal velocity increment along the direction of the line element, while V and W denote the two transverse increments.

To derive the equations for the increments, we consider the coarse-grained NS equations filtered at scale $\Delta \sim \ell$. Let $\widetilde{u}_i$ denote the filtered velocity field, and $\widetilde{A}_{ij} \equiv \partial_i\widetilde{u}_j$ denote the filtered velocity gradient, the equation for $\widetilde{A}_{ij}$ in a rotating frame of reference reads

$$\begin{aligned} D_t\widetilde{A}_{ij} = &-\widetilde{A}_{ik}\widetilde{A}_{kj} - 2\varepsilon_{jkl}\Omega_k\widetilde{A}_{il} \\ &- \frac{2}{3}(Q + \Omega_k\widetilde{\omega}_k)\delta_{ij} + H_{ij}. \end{aligned} \tag{3}$$

where $D_t \equiv \partial/\partial t + \widetilde{u}_j\partial_j$ is the material derivative in the filtered velocity field. The second term on the right-hand side (RHS) comes from the Coriolis force. $H_{ij} \equiv (-\partial^2_{ij}\widetilde{p} - \partial^2_{ik}\tau_{kj} + \nu\nabla^2\widetilde{A}_{ij}) - \frac{1}{3}\delta_{ij}(-\nabla^2\widetilde{p} - \partial^2_{mk}\tau_{km})$ is the anisotropic part of the pressure, subgrid-scale (SGS) stress, and viscous stress Hessian [27, 35]. The first term in the second line represents the corresponding isotropic part. $\widetilde{p}$ is the filtered pressure, $\tau_{ij} \equiv \widetilde{u_iu_j} - \widetilde{u}_i\widetilde{u}_j$ is the SGS stress, $\widetilde{\omega}_i \equiv (\nabla \times \widetilde{\mathbf{u}})_i$ is the filtered vorticity, and $Q \equiv -\widetilde{A}_{mn}\widetilde{A}_{nm}/2$ is the second tensor invariant of the filtered velocity gradient [27].

According to the Kolmogorov phenomenology, the contributions to the velocity increment $\delta\mathbf{u}$ mainly come from the motions around the scale ℓ. Therefore,

we have $\delta\mathbf{u} \approx \delta\widetilde{\mathbf{u}} \equiv \widetilde{\mathbf{u}}(\mathbf{x}+\ell\hat{\mathbf{r}},t) - \widetilde{\mathbf{u}}(\mathbf{x},t)$, given that $\Delta \sim \ell$. Since the filtered velocity field is smooth over the scales $\sim \ell$, we use linear approximations, and obtain

$$\delta\widetilde{u}_i \approx \ell\hat{\mathbf{r}}\cdot\nabla\widetilde{u}_i = \ell\hat{r}_j\partial_j\widetilde{u}_i = \ell\hat{r}_j\widetilde{A}_{ji}. \tag{4}$$

As a consequence, $U \approx \delta\widetilde{\mathbf{u}}\cdot\hat{\mathbf{r}} \approx \ell\widetilde{A}_{ij}\hat{r}_i\hat{r}_j$. Working out the expressions for V and W in a similar way, we find that the increments can be written as

$$U = \ell\widetilde{A}_{ji}\hat{r}_j\hat{r}_i,\ V = \ell\widetilde{A}_{ij}\hat{r}_i\hat{s}_j,\ W = \ell\widetilde{A}_{ij}\hat{r}_i\hat{t}_j. \tag{5}$$

Based on Eq. (5), the equations for the velocity increments can be derived from the equation for the filtered velocity gradient $\widetilde{A}_{ij}$ and those for the direction vectors. Using the evolution equation of the line element $D_t r_i = \widetilde{A}_{ji}r_j$, the equations for the direction vectors can be deduced from their definitions given in Eq. (1). In doing so, one finds that

$$D_t\hat{\mathbf{r}} = V\ell^{-1}\hat{\mathbf{s}} + W\ell^{-1}\hat{\mathbf{t}}, \tag{6}$$

$$D_t\hat{\mathbf{s}} = V\ell^{-1}(\cot\theta\hat{\mathbf{t}} - \hat{\mathbf{r}}), \tag{7}$$

$$D_t\hat{\mathbf{t}} = -\cot\theta V\ell^{-1}\hat{\mathbf{s}} - W\ell^{-1}\hat{\mathbf{r}}. \tag{8}$$

Angle θ in the equations is the angle between the line element $\mathbf{r}$ and the rotation axis $\mathbf{k}$, which evolves according the following equation:

$$D_t\theta = -W\,\ell^{-1}. \tag{9}$$

With Eqs. (6-8) and Eq. (3), the equations for the velocity increments can then be derived from the definitions (Eq. 5). After some algebra, the final equations are obtained as follows:

$$\begin{aligned} D_tU =& -U^2\ell^{-1} + V^2\ell^{-1} + W^2\ell^{-1} + 2\Omega V\sin\theta \\ & - \frac{2}{3}Q\ell - \frac{2}{3}\Omega_k\widetilde{\omega}_k\ell + \ell H_{ij}\hat{r}_i\hat{r}_j, \end{aligned} \tag{10}$$

$$\begin{aligned} D_tV =& -2UV\ell^{-1} + WV\ell^{-1}\cot\theta \\ & - 2\Omega(U\sin\theta - W\cos\theta) + \ell H_{ij}\hat{r}_i\hat{s}_j, \end{aligned} \tag{11}$$

$$\begin{aligned} D_tW =& -2UW\ell^{-1} - V^2\ell^{-1}\cot\theta - 2V\Omega\cos\theta \\ & + \ell H_{ij}\hat{r}_i\hat{t}_j. \end{aligned} \tag{12}$$

The equations describe the Lagrangian evolution of the velocity increments over the displacement ℓ. The most prominent feature of the equations is that the nonlinear interaction between the velocity increments as well as the Coriolis force are in closed form. Therefore the system is particularly suitable for examining the interplay between these two physical factors. On the other hand, the H_{ij}, Q and the $\Omega_k\widetilde{\omega}_k$ terms are not closed in the equations. To formulate a model that can be used to simulate rotating turbulence, models for the unclosed terms need to be developed. Several models for H_{ij} have been constructed in the context of the stochastic models for the velocity gradient [30, 33], which can be taken as the

basis for this purpose. Similarly, Q and $\Omega_k\widetilde{\omega}_k$ are closed if we were to work with a stochastic model for the full velocity gradient. However, as we have mentioned, our goal is to gain insights into the dynamics behind the observations regarding the non-Gaussian statistics of the velocity increments, rather than building a model for simulation. We thus choose to employ a simple restricted-Euler-type closure to handle the unclosed terms, and focus our attention on understanding the effects of the closed nonlinear terms and the Coriolis force. This approach is partly justified by the successes of previous research based on similar closure strategies. As will be shown soon, the resulted model will also be checked against DNS data, which confirms that the resulted system indeed captures significant part of the dynamics of Navier-Stokes turbulence.

Thus, following the idea of the restricted Euler approximation [26, 27], we set H_{ij} as well as $\Omega_k\widetilde{\omega}_k$ to zero in Eqs. (10-12). The term proportional to Q represents the part of the nonlinear self-interaction that is balanced by pressure to maintain incompressibility. As is shown in [35], part of the Q term is in closed form in terms of the velocity increments. To see this, note that in the local coordinate frame (see Fig. 1), the matrix $\widetilde{A}_{ij}$ can be written as

$$\widetilde{\mathbf{A}} = \begin{bmatrix} \widetilde{A}_{rr} & \widetilde{A}_{rs} & \widetilde{A}_{rt} \\ \widetilde{A}_{sr} & \widetilde{A}_{ss} & \widetilde{A}_{st} \\ \widetilde{A}_{tr} & \widetilde{A}_{ts} & \widetilde{A}_{tt} \end{bmatrix}, \tag{13}$$

where $\widetilde{A}_{rr} = U/\ell$, $\widetilde{A}_{rs} = V/\ell$, and $\widetilde{A}_{rt} = W/\ell$, according to Eq. (5). $\widetilde{A}_{tt} = -\widetilde{A}_{rr} - \widetilde{A}_{ss} = -U/\ell - \widetilde{A}_{ss}$ due to incompressibility. Since Q is a tensor invariant, it is the same for different projections of $\widetilde{A}_{ij}$. Based on the above projection, simple calculation shows that $Q = -\ell^{-2}U^2 + Q^-$, where the first term comes from $\widetilde{A}_{rr}^2$ and part of $\widetilde{A}_{tt}^2$, and Q^- contains the other unclosed terms [35]. We retain the first term while neglecting Q^-. Applying these approximations (neglecting H_{ij}, $\Omega_k\widetilde{\omega}_k$ and Q^-), the final restricted-Euler-type model is given as:

$$D_tU = -\frac{1}{3}U^2\ell^{-1} + V^2\ell^{-1} + W^2\ell^{-1} + 2\Omega V\sin\theta \tag{14}$$

$$D_tV = -2UV\ell^{-1} + WV\ell^{-1}\cot\theta - 2\Omega(U\sin\theta - W\cos\theta) \tag{15}$$

$$D_tW = -2UW\ell^{-1} - V^2\ell^{-1}\cot\theta - 2V\Omega\cos\theta. \tag{16}$$

The above equations, together with Eq. (9), form a closed system. The system describes the effects of the nonlinear interaction terms and the Coriolis force on the evolution of the velocity increments.

When $\Omega = 0$, i.e., when there is no rotation, Eqs. (14-16) can be compared with the advected delta-vee system in [35] and [36]. The advected delta-vee system is a system of two equations for δu and δv. In present notations, δu and δv correspond to U and $(V^2+W^2)^{1/2}$, respectively. From Eqs. (14-16), one can easily derive the equations for δu and δv. When $\Omega = 0$, the equations are the same as the delta-vee system. Therefore current system is a generalization to

the advected delta-vee system. As having been pointed out in [35], the advected delta-vee system captures a number of essential mechanisms that are responsible for the non-Gaussian statistics in the small scales of turbulence. The current system also contains these mechanisms. It is well-known that, in turbulence in three spatial dimensions, the longitudinal velocity increment develops a negative skewness, which is a signature of the energy cascade process (see e.g. [18]). Eq. (14) shows that the first term on the RHS, being always negative, will always amplify the negative fluctuations in U. Therefore, this term produces a self-amplification mechanism for the negative fluctuations in the longitudinal velocity increments, and is the source of the negative skewness. Physically, it represents an effect similar to the front-steeping process observed in the Burgers' equation [37]. On the other hand, numerous observations show that the transverse velocity increments frequently experience violent fluctuations. As a consequence, the probability density functions (PDF) of the transverse velocity increments display exponential or stretched-exponential tails, compared with the Gaussian distribution [18, 38]. This trend can be qualitatively explained by the first term on the RHS of Eq. 15, and also the first term on the RHS of Eq. 16. These terms show that, when the longitudinal velocity increment U is negative, exponential growth, and hence strong fluctuations, in the transverse increments V and W can be generated. This mechanism for generating strong fluctuations in transverse velocity increments is termed the 'cross amplification' mechanism in [35]. In rotating turbulence, these mechanisms are accompanied by the Coriolis force, as is shown by Eqs. (14-16). It is the goal of this paper to understand the interaction between the nonlinear terms and the Coriolis force based on the above model equations. (For more analyses concerning the nonlinear interaction between the velocity increments in Eqs. (14-16) in non-rotating turbulence, we refer the readers to [35, 36].)

Given the drastic approximations that we have made, it is desirable to check to what extent the model captures the dynamics of the Navier-Stokes turbulence. We thus compute the correlation between the rates of changes of the velocity increments predicted from the model and the actual rates of changes resulted from the full Navier-Stokes dynamics, using a DNS data set. The former is calculated from the right-hand sides of Eqs. (14-16), while the latter is calculated by following the evolution of line elements , as well as the velocity increments over the line elements, in filtered DNS velocity fields. In what follows, the latter results are referred to as the 'exact' results. The technical details of the analysis have been explained in [35]. The DNS data are generated by solving the NS equations with pseudospectral method and Adam-Bashforth second order time integration. The flow is forced at wavenumbers $|\mathbf{k}| < 3$, injecting energy at a constant rate. 256^3 grids are used. The Coriolis force is integrated exactly using integrating factor, based on the helical decomposition of the Fourier modes [4]. Initial velocity field is taken from a fully developed isotropic velocity field obtained from pre-simulations without rotation. The initial Reynolds number $Re_\lambda \equiv u'\lambda/\nu \approx 114$, where $u' = 0.66$ is the initial root-mean-square (rms) velocity fluctuation and λ the Taylor length scale. The initial Rossby number $Ro \equiv u'/\Omega L$ is set to 0.2, where $L = \pi$ is the forcing scale. The data used in

the following analysis are taken at a time when an approximate k^{-2} spectrum is observed [5]. Fig. 2 shows the energy spectra for the data with or without rotation, compensated with k^2.

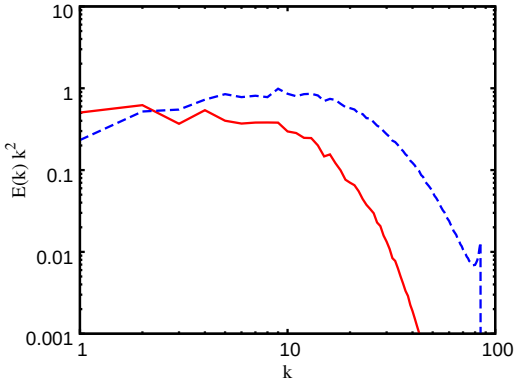

Figure 2: Energy spectra compensated with k^2. Solid line: with rotation; dashed line: initial spectrum (without rotation).

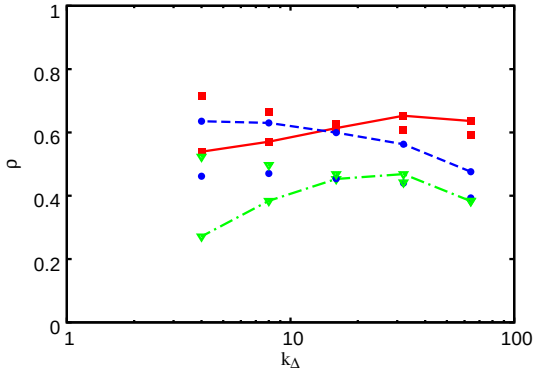

Figure 3: Correlation between the rates of changes of the velocity increments predicted from model [Eqs. (14-16)] (model results) and those calculated by tracking the Lagrangian evolution of the material lines and the increments (the exact values). Lines with symbols: $Ro = 0.2$; symbols only: without rotation. Squares: D_tU, circles: D_tV, gradients: D_tW. $k_\Delta = \pi/\Delta$.

Fig. 3 plots the correlation coefficients for the rates of changes of the increments at several filter scale Δ. The results for rotating turbulence are plotted with lines with symbols. The results obtained from the DNS data of non-rotating turbulence are also plotted with symbols for comparison. Averaging is taken over all the grid points and for $\hat{\mathbf{r}}$ along the two coordinate directions in the plane normal to the rotating axis. Therefore $\theta = \pi/2$ and the W component of the increment is in the direction of the rotation axis. ℓ is taken as the same as Δ in each case. In rotating turbulence, the figure shows that, for D_tU and D_tV, the

correlation coefficients are close to 0.6, with only small variation over different scales. For D_tW, the correlation coefficient is somewhat smaller. At small scales (with larger $k_\Delta \equiv \pi/\Delta$), the coefficient ranges between 0.4 and 0.5. At larger scales, the correlation tends to decrease. Since the W component points along the rotation axis, the Coriolis force affects its evolution indirectly through the pressure field. Since the effects of pressure have only been partially accounted for (by including part of the Q term), it is probably the reason why the correlation between the model for D_tW and the real dynamics is relatively weaker at large scales, where the effects of rotation becomes stronger. Nevertheless, Fig. 3 shows that the model captures a significant part of the dynamics in rotating turbulence, particularly for the U and V components. The results suggest that the model is a better representation of the dynamics of the Navier-Stokes turbulence for moderate rotation rates.

For non-rotating turbulence, the correlation coefficient for D_tU is about the same as in rotating turbulence at smaller scales. The values increase slightly at larger scales, whereas in rotating turbulence the values decreases slightly. The values for D_tV and D_tW are almost the same at small scales, as one would expect in isotropic turbulence. At larger scales, some small difference can be observed, probably due to the residual anisotropy in large scales. The coefficients for D_tV and D_tW in non-rotating turbulence are about the same as the values for D_tW in rotating turbulence. Interestingly, in rotating turbulence, the correlation coefficients for D_tV are bigger that its values in non-rotating turbulence. To summarize, the correlation coefficients in non-rotating turbulence show some differences in both qualitative and quantitative aspects, but the level of correlation is still significant. The observations are consistent with the results reported in our previous publications [35, 36].

Fig. 4 shows the joint PDF of the exact values of D_tV and the values calculated from the model (solid lines). Also shown is the conditional average $\langle D_tV_{\text{Model}}|D_tV_{\text{DNS}}\rangle$ (dashed line). The data are calculated at $\Delta = \ell = 16\delta x$, where $\delta x = \pi/128$ is the grid size. Note that, for a perfect model, the joint PDF would fall entirely on the diagonal. For our model, the joint PDF spreads around the diagonal to some extent. The model appears to somewhat over-predict the probabilities of large fluctuations. Nevertheless, the joint PDF clearly shows significant correlation between the model and the exact values. Similar trends can be observed in the joint PDF for D_tU (not shown). The conditional average, shown by the dashed line, is consistent with the results for joint PDF. The curve is only slightly steeper than the diagonal. The results for D_tW are shown in Fig. 5. One can see that the joint PDF for D_tW spreads out relatively wider around the diagonal, which explains the somewhat lower correlation coefficient for D_tW observed in Fig. 3. The conditional average is a bit shallower than the diagonal, indicating that, on average, the model tends to underestimate the rate of change of W. Overall, the joint PDFs show significant correlation between the model predictions and the exact values, complementing the results for correlation coefficients.

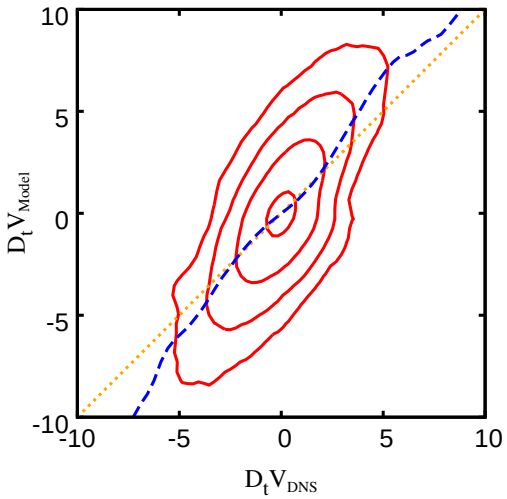

Figure 4: Joint PDF of $D_tV_{\rm DNS}$ and $D_tV_{\rm Model}$ (solid lines) and the conditional average $\langle D_tV_{\rm Model}|D_tV_{\rm DNS}\rangle$ (dashed line). $D_tV_{\rm DNS}$ is the rate of change of the transverse velocity increment V calculated by following the Lagrangian evolution of velocity increment over a line element. $D_tV_{\rm Model}$ is the rate of change given by the model expression calculated using DNS data. Starting from inside, the levels are 10^{-1}, 10^{-2}, 10^{-3}, 10^{-4}. The dotted line is the diagonal.

3. Numerical results and discussions

In this section we study the evolution of the velocity increments predicted by the model, starting from initial Gaussian random condition. U, V and W are initialized as Gaussian random numbers with zero mean and unit variance, so that the velocity scale is $u' = 1$. Initially the material line elements point to different directions with equal probabilities, so that $\cos\theta$ is uniformly distributed in $[-1, 1]$. At any time t, statistics are accumulated from the evolving ensemble. Eqs. (9), (14-16) are solved numerically, using the same method as in [35]. As noted in [35, 36], because the line elements tend to concentrate in the stretching directions of the velocity gradient, the statistics of the evolving ensemble will be different from the statistics taken over random directions. To compare the results with the latter, the measure correction procedure described in [35, 36] is applied. Experimental and DNS results have so far only been reported for increments defined in the perpendicular plane. To compare with these results, we plot the PDFs of U, V, and W conditioned on $\cos\theta = \cos 90^\circ = 0$, corresponding to the case where the line elements lie in the perpendicular plane. We set the displacement $\ell = 1$, and define the Rossby number as $Ro \equiv u'/\Omega\ell = 1/\Omega$.

As a base case for comparison, we first consider the results when $\Omega = 0$. Fig. 6 shows the PDFs of U at several times ranging from $t = 0$ to $t = 0.24$. The PDFs of V and W at the same times are shown in Fig. 7. Note that the time scale defined with initial parameters is $\ell/u' = 1$. Thus the figures show that the PDFs of the longitudinal velocity increments develop negative skewness rapidly.

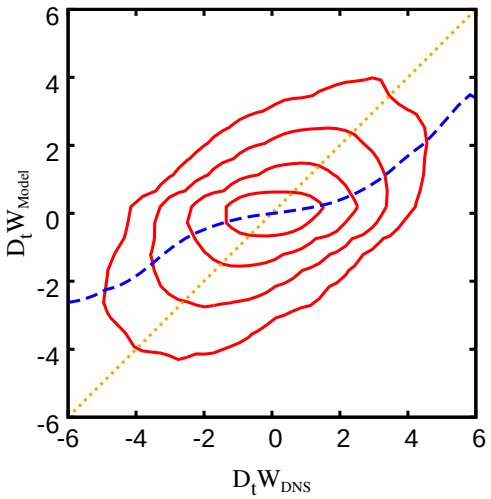

Figure 5: Same as Fig. 5, but for $D_t W$.

At the same time, exponential or stretched exponential tails are built up in the PDFs of the transverse velocity increments. These trends reproduce the results of [35], and are qualitatively consistent with the well-known observations in turbulence, as having been shown in [35]. The results confirm numerically that the current system is consistent with the advected delta-vee system derived in [35]. Fig. 7 shows that, as expected, the PDFs of V and W are nearly identical to each other, except for some small differences due to statistical fluctuations.

We now consider the results when rotation is present. The first results are concerned with the effects of rotation on the skewness of the longitudinal velocity increments. Figs. 8 and 9 show the PDFs of U at Rossby number $Ro = 0.1$ and 0.05, respectively. Different curves correspond to different times, shown with the same legend as in Fig. 6. Comparing the two figures with Fig. 6 (for which $\Omega = 0$), one can see that the asymmetry in the PDFs of U shown in Figs. 8 and 9 is smaller. In other words, the model predicts that the skewness in U is reduced when rotation is imposed. For $Ro = 0.05$, the PDFs are actually very close to Gaussian.

The shapes of the PDFs can be measured quantitatively by the skewness and the flatness. The skewness of a random variable X is defined as $S_X \equiv \langle (X - \langle X \rangle)^3 \rangle / \langle (X - \langle X \rangle)^2 \rangle^{3/2}$, where $\langle \cdots \rangle$ denotes the ensemble average. The flatness of X is defined as $F_X \equiv \langle (X - \langle X \rangle)^4 \rangle / \langle (X - \langle X \rangle)^2 \rangle^2$. Fig. 10 shows the time evolutions of $-S_U$, calculated by integrating the conditional PDFs [35]. Data for several Ro numbers are shown. When there is no rotation, $-S_U$ increases over time, and take a value around 0.5 at $t = 0.24$ (solid line). When rotation rate increases (the Ro number decreases), the increase of $-S_U$ over time is suppressed. $-S_U$ appears to oscillate around zero, with an amplitude that decreases with the Ro number. With $Ro = 0.025$, i.e., strong rotation, the

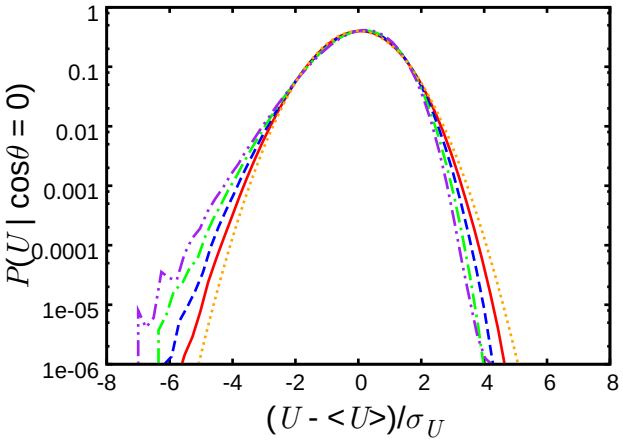

Figure 6: Evolution of the conditional PDFs of U when there is no rotation ($Ro = \infty$). Dotted line: initial Gaussian distribution; solid line: $t = 0.06$; dashed: 0.12; dash-dotted: 0.18; dash-double-dotted: 0.24. σ_U is the root-mean-square value of the longitudinal velocity increment U.

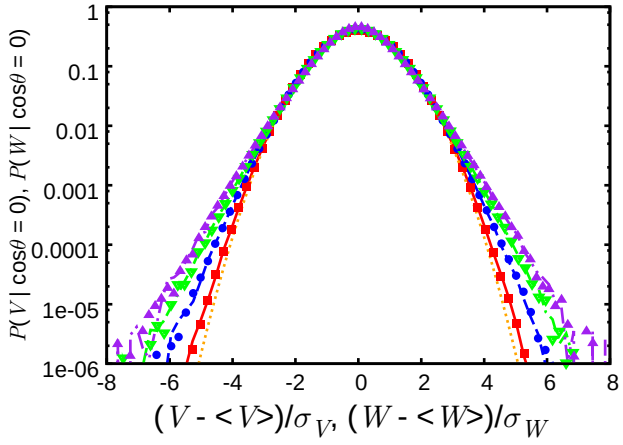

Figure 7: Evolution of the conditional PDFs of V (lines) and W (symbols) when there is no rotation ($Ro = \infty$). Dotted line: initial Gaussian distribution; solid line and squares: $t = 0.06$; dashed line and circles: 0.12; dash-dotted line and gradients: 0.18; dash-double-dotted line and deltas: 0.24. σ_V and σ_W are the root-mean-square values of the velocity increments V and W, respectively.

skewness is essentially zero. Fig. 11 plots the flatness of U as a function of time, for several Ro numbers. Fig. 11 shows that the growth of the flatness of U over time is again suppressed when strong rotation is imposed. At $Ro = 0.1$, F_U stays at a value around 3.1 with little fluctuation. At $Ro = 0.05$ and 0.025, F_U is essentially equal to 3, the value for Gaussian distribution. A small value of F_U implies that large fluctuations happen with less probability. The

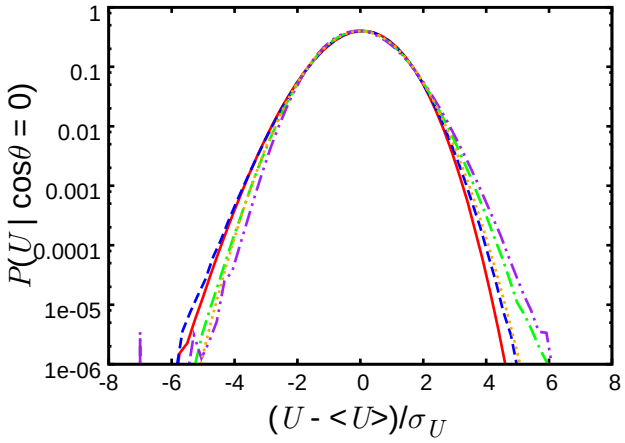

Figure 8: The conditional PDFs of U at Rossby number $Ro = 0.1$. Line legend is the same as in Fig. 6.

results thus indicate that strong rotation tends to reduce the appearance of large fluctuations in the longitudinal velocity increments. When $Ro = 0.2$ (not shown), however, the flatness appears to take somewhat larger values than in the case without rotation. The value reaches 3.8 at $t = 0.24$, compared with the value 3.5 when there is no rotation. The reason for this increase is not clear at present. Nevertheless, the overall prediction of the model is that, when strong rotation is imposed, both the skewness and flatness of the longitudinal velocity increment are weakened. This prediction is consistent with DNS and experimental results (see, e.g., [4, 9, 19]).

We now consider another interesting feature in rotating turbulence, the positive skewness in the cyclonic vorticity component (i.e., the vorticity component along the rotation axis). Observations in rotating turbulence have shown that the distribution of cyclonic vorticity displays positive skewness. As is summarized in section 1, the skewness varies with the Rossby number in a non-monotonic way, with a maximum reached at an intermediate Rossby number [13, 15]. Two main explanations have been proposed for the origin of the skewness. The anti-cyclonic vortices are shown to be unstable under the action of background rotation in [13]. The mechanism is proposed as an explanation for the positive skewness for the cyclonic vorticity component. On the other hand, [21] (see also [20]) shows that the initial growth rate of the skewness is proportional to the product between Ω and the mean vortex stretching. Since the mean vortex stretching is positive in isotropic turbulence, positive skewness will be generated when rotation is imposed.

As our model is developed for the velocity increments over a single line element, it does not contain sufficient information to determine the evolution of the vorticity. However, the V component is related to the cyclonic vorticity component ω_z when the line element is perpendicular to the rotation axis. For

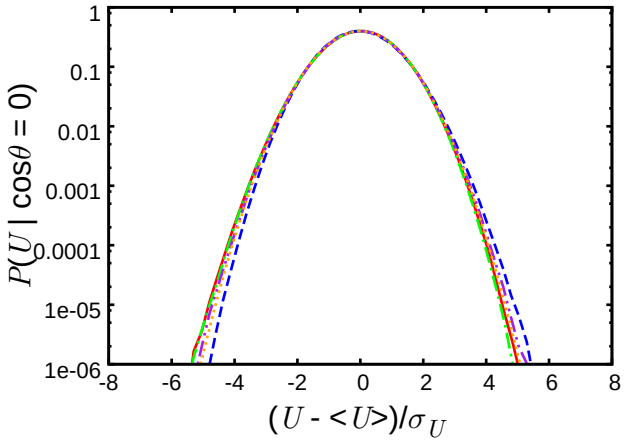

Figure 9: The conditional PDFs of U at Rossby number $Ro = 0.05$. Line legend is the same as in Fig. 6.

example, when the displacement ℓ is along the x direction, $\omega_z = V/\ell - \partial u_x/\partial y$, according to the definition in Eq. 5. Thus, one may conjecture that V will also display positive skewness in rotating turbulence. It is interesting to check if the model will be able to predict this behavior. Figs. 12, 13 and 14 give the PDFs of V predicted by the model, at Rossby number $Ro = 0.2$, 0.1, and 0.05, respectively. We recall that there is no skewness in V when the rotation rate is zero, as is demonstrated by Fig. 7. The PDFs of V at $Ro = 0.5$ (no shown) also display no visible skewness. However, Fig. 12 shows that strong positive skewness for V has been developed at $Ro = 0.2$, reminiscent of the positive skewness for the cyclonic vorticity component. Furthermore, Figs. 13 and 14 show that the skewness tends to decrease when the rotation rate is further increased. At $Ro = 0.05$, the PDFs show little deviation from the Gaussian distribution. Therefore, the development of the positive skewness is the strongest around $Ro = 0.2$. Fig. 15 gives the skewness of V as a function of time for several Rossby numbers. The skewness grows initially and then oscillates around a positive value. For comparison, a power-law $(\Omega t/2\pi)^n$, where $n = 0.75$, is also plotted in Fig. 15. The power law has been used to fit the initial growth of the skewness of the cyclonic vorticity component in [20]. Slightly different values for n are used in [9, 17]. Fig. 15 shows that the growth of the skewness of V is approximately algebraic, but with a rate slightly faster than the empirical power law. The maxima are reached at roughly the same values of $\Omega t/2\pi$ for the three Rossby numbers, and the values are between 0.2 and 0.3. The range of the values is similar to the one for the skewness of the cyclonic vorticity component documented in [20].

Finally, Fig. 16 shows the evolution of the flatness of V over time for different Rossby numbers. Similar to the flatness of the longitudinal component U, when the rotation rate increases, the development of the flatness over time

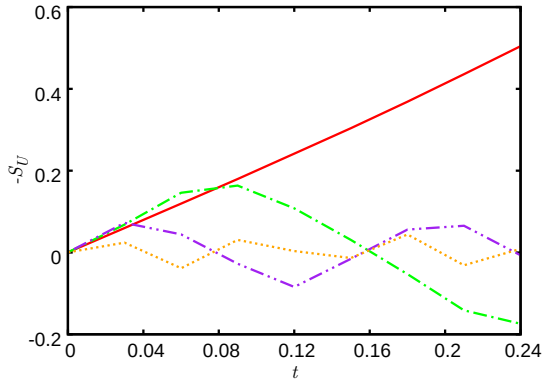

Figure 10: The evolution of $-S_U$, the magnitude of the skewness of the longitudinal velocity increment U, at Rossby number $Ro = \infty$ (solid line), 0.1 (dash-dotted), 0.05 (dash-double-dotted), 0.025 (dotted).

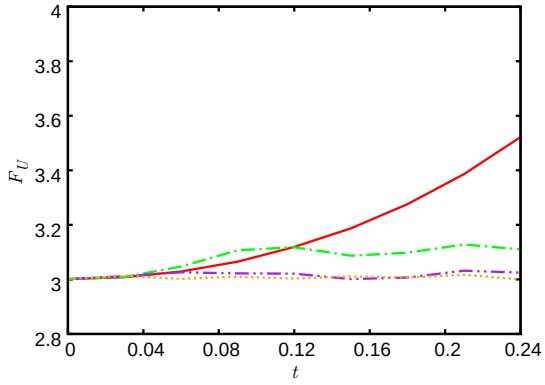

Figure 11: The evolution of F_U, the flatness of the longitudinal velocity increment U. Legend is the same as in Fig. 10.

is suppressed. The values of the flatness are smaller compared with the values when no rotation is present. At the smallest Rossby numbers $Ro = 0.05$ and 0.025, the flatness again stays at the Gaussian value 3, consistent with the results for the PDFs.

The above results demonstrate that the model is able to qualitatively reproduce several important trends observed in DNS and experiments. Besides, the positive skewness in the transverse velocity increment in the plane perpendicular to the rotation axis has not been reported before. Because of the simplicity of the model, it is possible to understand the effects of each term in the equations, and explain the observations in terms of the interplay between different terms, as we will show now. First of all, when the Rossby number is small (rotation is strong), the Coriolis forces in Eqs. (14) and (15) dominate. If we neglect the nonlinear terms, the evolution of U and V is decoupled from W, when the

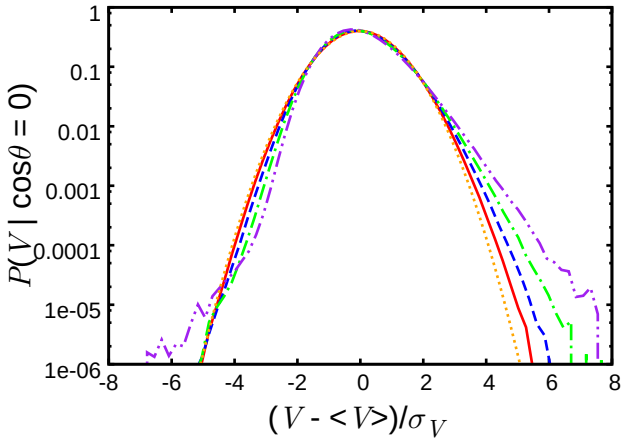

Figure 12: The evolution of the conditional PDFs of V at Rossby number $Ro = 0.2$. Legend is the same as in Fig. 6.

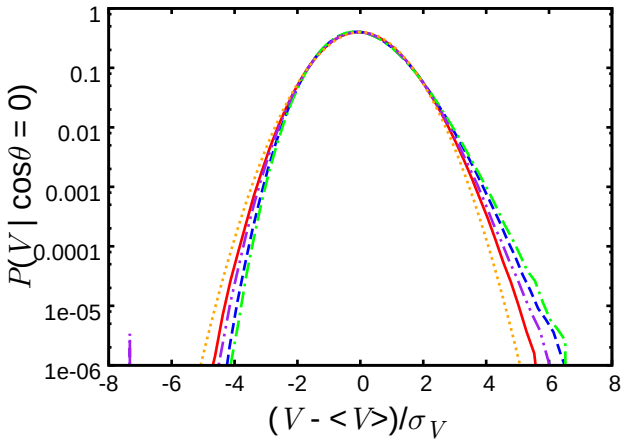

Figure 13: The evolution of the conditional PDFs of V at Rossby number $Ro = 0.1$. Legend is the same as in Fig. 6.

displacement is perpendicular to the rotation axis. In this limit, Eqs. (14) and (15) are simplified to

$$D_t U = 2\Omega V, \;\; D_t V = -2\Omega U. \tag{17}$$

It is trivial to show that an energy-like quantity $U^2 + V^2$ is conserved by the system. Thus, U and V are bounded by initial conditions and non-Gaussian tails are prohibited. This explains the observations in Figs. 9 and 14 that, when Ro is small, the negative skewness in U is reduced and the PDFs of both U and V stay close to Gaussian.

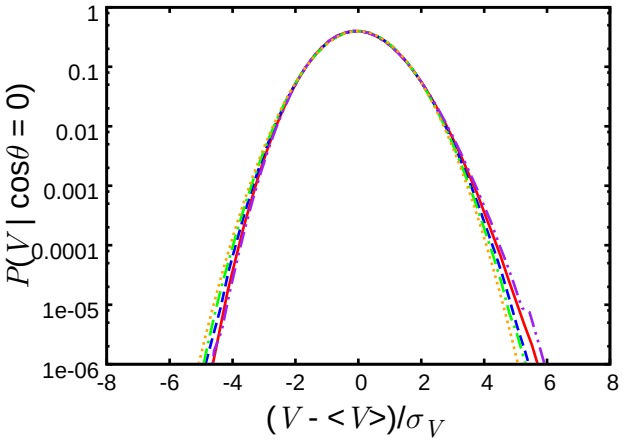

Figure 14: The evolution of the conditional PDFs of V at Rossby number $Ro = 0.05$. Legend is the same as in Fig. 6.

The origin of the positive skewness of V at moderate Ro numbers can also be understood from Eqs. (14-16). As we mentioned before, the positive skewness of V is related to the positive skewness of the cyclonic vorticity component ω_z. Therefore, the following discussion also applies qualitatively to the latter. We will compare the explanations based on our model with those proposed in the literature. At moderate Ro numbers, the PDFs of U still display significant negative skewness, albeit already weakened by rotation. When U is negatively skewed, the Coriolis force $-\Omega U$ in the equation for V [Eq. (15)] has a positive skewness. Thus, according to Eq. (15), the Coriolis force tends to produce positive skewness in V. Since the negative skewness in U is an indication of positive vortex-stretching in turbulence, this mechanism resembles the one identified by [21] (see also [20]), where the skewness of the vertical vorticity component is explained in terms of the interaction between vortex stretching and the Coriolis force. On the other hand, due to the Coriolis force ΩV in the equation for U [Eq. (14)], negative fluctuations in V tend to increase negative skewness of U. Again, because of the Coriolis force in the equation for V, negative skewness in U will have an effect to promote the positive fluctuations in V and reduce its negative fluctuations. In other words, negative fluctuations in V tend to self-diminish, which thus also contributes to positive skewness in V. In effects, this mechanism affects the skewness of V in a way similar to the destablization of anti-cyclonic vortices due to background rotation. The latter is proposed in [13] to explain the positive skewness of the cyclonic vorticity component. Therefore, our model suggests that both the mechanisms proposed in the literature contribute their parts to the positive skewness in the cyclonic vorticity component in rotating turbulence. However, it may not be necessary to invoke any coherent structures in the flows to explain the phenomenon.

The above analysis implies that the magnitude of the skewness in V depends

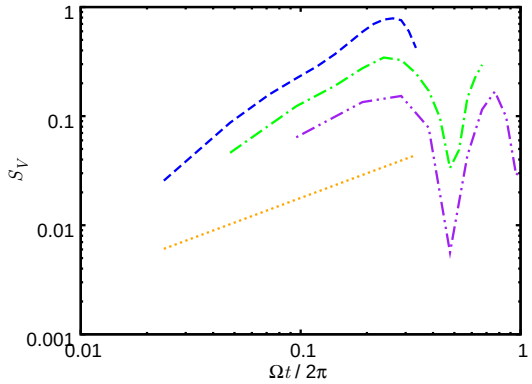

Figure 15: The growth of the skewness of V over time for $Ro = 0.2$ (dashed line), 0.1 (dash-dotted), and 0.05 (dash-double-dotted). The dotted line is $(\Omega t/2\pi)^{0.75}$.

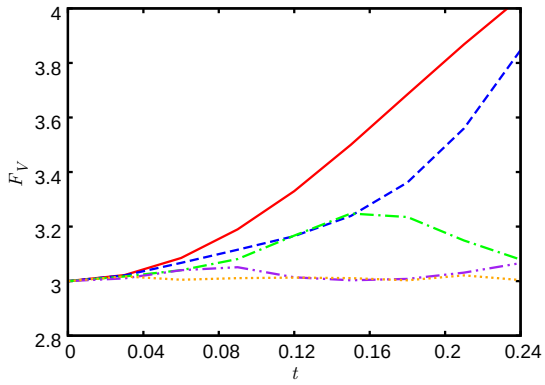

Figure 16: The growth of the flatness of V over time for $Ro = \infty$ (solid line), 0.2 (dashed line), 0.1 (dash-dotted), 0.05 (dash-double-dotted), and 0.025 (dotted).

on both the rotation rate and the magnitude of the negative skewness in U. When rotation is so strong that the nonlinear self-interaction is negligible, the skewness in U is suppressed, and so is the positive skewness in V. At very large rotation rates, the distribution of U becomes symmetric, as in Fig. 9. As a result, V also becomes symmetric.

The dynamics of U and V can also be qualitatively understood via the phase portraits of the system. To simplify the analysis, we set W as zero in the equations of U and V and consider the case when the displacement ℓ is perpendicular to the rotation axis. The resulted system reads

$$D_t U = -\frac{1}{3}U^2\ell^{-1} + V^2\ell^{-1} + 2\Omega V, \quad D_t V = -2UV\ell^{-1} - 2\Omega U. \tag{18}$$

Integrating the equation, one can show that the system has the following invari-

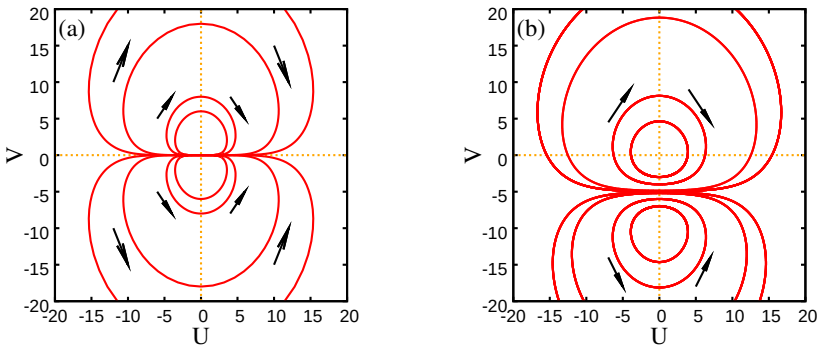

Figure 17: The phase portrait for the approximate dynamics of (U, V) given by Eq. (18). (a): $\Omega = 0$ ($Ro = \infty$), (b): $\Omega = 5$ ($Ro = 0.2$). The phase portraits are separated into two parts by the horizontal line $V = -\Omega\ell$. In the upper part, the orbits point in the clockwise direction, while in the lower part, the orbits point in the counter-clockwise direction, as indicated by the arrows.

ant

$$H(U,V) = \left[U^2 + \frac{3}{5}(V+\Omega\ell)^2 + 3(\Omega\ell)^2\right](V+\Omega\ell)^{-1/3}. \tag{19}$$

Several contours of $H(U, V)$, which are also the trajectories of (U, V) in the phase plane, are shown in Fig. 17, for (a) $Ro = \infty$ and (b) $Ro = 5$. When there is no rotation (i.e., $Ro = \infty$), the expression of $H(U, V)$ is reduced to $(U^2 + 3V^2/5)V^{-1/3}$, which is the same as the expression in [36] for the invariant of the advected delta-vee system (in three spatial dimensions). In this case, the origin is a degenerated fixed point (see Fig. 17a). The trajectories show that, when the phase points move towards the negative U direction due to the self-amplification mechanism, the magnitude of V must increase drastically. This behavior is a consequence of the cross amplification mechanism. Therefore, the phase portrait provides an intuitively straightforward picture for the dynamics of the system. When rotation is imposed, the phase portrait is shifted downwards, as is shown in Fig. 17b. Meanwhile, two centers appear at $(0, 0)$ and $(0, -2\Omega\ell)$ (Note that point $(0, -\Omega\ell)$ is not a fixed point for $\Omega \neq 0$). The phase portraits allow an intuitive understanding of the effects of rotation on the skewness in V. When rotation is absent, the portrait is symmetric with respect to $V = 0$, therefore no skewness is generated in V. When rotation is present, the phase portrait is no longer symmetric. Fig. 17b shows that the values of V between $-\Omega\ell$ and zero will be increased when $U < 0$, and decreased when $U > 0$. When U has a negative skewness, the tendency for V to increase prevails that for V to decrease. The net effect is to increase V and hence generate the positive skewness in V. When the values of V fall between $-\Omega\ell$ and zero, the phase points move in the clockwise direction along the trajectories. Therefore, there is a tendency to generate negative skewness in U and, subsquently positive skewness in V. This tendency corresponds to the self-diminishing effects of negative fluctuations of V mentioned above. Therefore, the physical picture

emerging from the phase portrait is consistent with our previous analysis based on the dynamical equations. Even though the phase portraits are based on the simplified system, the qualitative picture is expected to be the same for the full system as far as the dynamics of U and V is concerned.

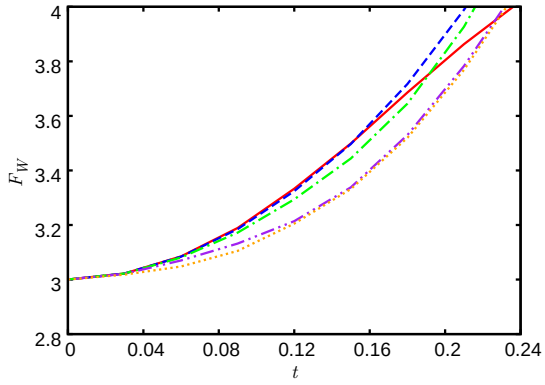

Figure 18: The evolution of the flatness of W. Legend is the same as in Fig. 16.

Finally, we briefly discuss the results for the other transverse velocity increment W. Fig. 18 shows the flatness of W as a function of time, for several Rossby numbers. It can be seen that, even with strong rotation such that $Ro = 0.025$, the flatness still increases over time, departing from the Gaussian value 3. The rate of increase of the flatness is somewhat slower initially, compared with the case without rotation (solid line), resulting in smaller values initially. But the difference is small. The general observation about the results of W is that the effects of rotation on W are relatively weak. The DNS analysis in [19] seems to show similar trends for the gradients of the velocity components. In particular, it is found in [19] that, while the flatness of the transverse gradients of all velocity components is reduced by rotation, the flatness of the transverse gradients of the vertical velocity component (corresponding to W) sustains a larger value compared with other components. In other words, the effects of rotation is weaker on the vertical component. The model prediction on W is qualitatively consistent with this observation.

4. Conclusions

To summarize, we have derived a system of equations describing the evolution of velocity increments over a fixed distance on an evolving material element in rotating turbulence. The system extends the ideas presented in previous papers [35, 36] to include the effects of rotation. To do so, a Lagrangian local coordinate frame is defined. As a result, the nonlinear interaction between the increments as well as the Coriolis force are closed in the system, which thus allows detailed investigations of their effects. Focusing on the dynamical effects of the nonlinear interaction terms as well as the Coriolis force on the evolution

of the velocity increments, we employ a simple restricted-Euler-type closure to the system, neglecting the anisotropic pressure Hessian and a few other terms. The resulted model is used to elucidate the basic dynamical mechanisms behind the evolution of the non-Gaussian statistics of velocity increments. We show via *a priori* analyses of DNS data that the model captures important dynamics in the Navier-Stokes equations. Numerical experiments starting from Gaussian initial conditions show that the model reproduces a number of observations regarding the effects of rotation on the development of the non-Gaussian statistics in the increments. In particular, the model reproduces the trend that the negative skewness in the longitudinal velocity increments is attenuated by strong rotation. The model also predicts that the transverse increment in the plane perpendicular to the rotation axis will develop positive skewness, and the magnitude of the skewness depends on the rotation rate non-monotonically. This behavior of the velocity increment is closely related to the positive skewness of the cyclonic vorticity component, but has not been reported before. Taking advantage of the simplicity of the model, we identify the specific processes responsible for the observations, which helps clarify the roles of different explanations proposed in the literature.

We conclude that the model is useful to assist our understanding of the effects of rotation. Nevertheless, a number of terms have been omitted. Appropriate models for these terms need to be developed in order to obtain stationary statistics and make quantitative comparisons with DNS and experimental data. Our preliminary *a priori* DNS analyses reported above have provided useful information as to the overall effects of the neglected terms. However, the roles of each individual term need to be understood. As a first step, one could perform a conditional statistical analysis of the unclosed terms. If we consider the joint PDF of the velocity increments, the unclosed terms will appear as conditional averages for given values of the velocity increments. These conditional averages determine the probability fluxes generated by the unclosed terms. DNS analyses of the conditional averages will shed light on the specific effects of each unclosed term. For the advected delta-vee system in non-rotating turbulence, an analysis of this kind has been conducted [39]. One interesting observation is that the pressure Hessian displays distinctively different behaviors from the viscous and SGS stress terms. The viscous and SGS stresses serve as damping terms so that the probability fluxes produced by these term terms point to the origin in the phase plane for the velocity increments. On the other hand, the stream traces of the probability flux vector field produced by the pressure Hessian originate from a source near the origin, follow anti-clockwise circular paths and terminate at a sink near the origin. Therefore, the modelling of pressure Hessian and the other terms requires different treatments. This is our on-going work. For the system reported here, the behaviors of the conditional averages will be different due to the presence of rotation. Furthermore, the quantity $\Omega_k\omega_k$ appears as a new term. Thus it is of considerable interests to look into the statistics of these quantities using DNS or experimental data of rotating turbulence. The information obtained from such analyses would be useful resources for the modelling of the unclosed terms. These could be the next steps in the research along this

line.

5. Acknowledgement

The author wishes to thank L. Chevillard, G. L. Eyink, C. Meneveau, and K. Ohkitani for helpful discussions.

[1] H. P. Greenspan, The theory of rotating fluids, Cambridge University Press, 1968.

[2] P. Sagaut, C. Cambon, Homogeneous Turbulence Dynamics, CUP, 2008.

[3] N. N. Mansour, T.-H. Shih, W. C. Reynolds, The effects of rotation on initially anisotropic homogeneous flows, Phys. Fluids A 3 (1991) 2421.

[4] C. Cambon, N. N. Mansour, F. S. Godeferd, Energy transfer in rotating turbulence, J. Fluid Mech. 337 (1997) 303–332.

[5] P. K. Yeung, Y. Zhou, Numerical study of rotating turbulence with external forcing, Phys. Fluids 10 (1998) 2895.

[6] L. M. Smith, F. Waleffe, Transfer of energy to two-dimensional large scales in forced, rotating three-dimensional turbulence, Phys. Fluids 11 (1999) 1608.

[7] X. Yang, J. A. Domaradzki, Large eddy simulations of decaying rotating turbulence, Physics of Fluids 16 (11) (2004) 4088–4104. doi:10.1063/1.1790452.

[8] Q. Chen, S. Chen, G. L. Eyink, D. D. Holm, Resonant interactions in rotating homogeneous three-dimensional turbulence, J. Fluid Mech. 542 (2005) 139–164.

[9] C. Morize, F. Moisy, M. Rabaud, Decaying grid-generated turbulence in a rotating tank, Phys. Fluids 17 (2005) 095105.

[10] Y. Zhou, A phenomenological treatment of rotating turbulence, Phys. Fluids 7 (1995) 2092.

[11] F. Bellet, F. S. Godeferd, J. F. Scott, C. Cambon, Wave turbulence in rapidly rotating flows, J. Fluid Mech. 562 (2006) 83–121.

[12] M. Hossain, Reduction in the dimensionality of turbulence due to a strong rotation, Phys. Fluids 6 (1994) 1077–1080.

[13] P. Bartello, O. Mètais, M. Lesieur, Coherent structures in rotating three-dimensional turbulence, J. Fluid Mech. 273 (1994) 1–29.

[14] L. M. Smith, Y. Lee, On near resonances and symmetry breaking in forced rotating flows at moderate Rossby number, J. Fluid Mech. 535 (2005) 111–142.

[15] L. Bourouiba, P. Bartello, The intermediate rossby number range and two-dimensional-three-dimensional transfers in rotating decaying turbulence, J. Fluid Mech. 587 (2007) 139–161.

[16] P. A. Davidson, P. J. Staplehurst, S. B. Dalziel, On the evolution of eddies in a rapidly rotating system, J. Fluid Mech. 557 (2006) 135–144.

[17] P. J. Staplehurst, P. A. Davidson, S. B. Dalziel, Structure formation in homogeneous freely decaying rotating turbulence, J. Fluid Mech. 598 (2008) 81–105.

[18] U. Frisch, Turbulence: the legacy of A. N. Kolmogorov, Cambridge universtiy press, Cambridge, 1995.

[19] P. K. Yeung, J. Xu, K. R. Sreenivasan, Scaling properties in rotating homogeneous turbulence, Proceeding of FEDSM'03, 2003 4th ASME/JSME Joint Fluids Engineering Conference (2003).

[20] L. J. A. van Bokhoven, C. Cambon, L. Liechtenstein, F. S. Godeferd, H. J. H. Clercx, Refined vorticity statistics of decaying rotating three-dimensional turbulence, J. Turbulence 9 (2008) doi:10.1080/14685240701877271.

[21] J.-N. Gence, C. Frick, Birth of the triple correlations of vorticity in an homogeneous turbulence submitted to a solid body rotation, C. R. Acad. Sci. Paris 329 (2001) 351–356.

[22] C. N. Baroud, B. B. Plapp, H. L. Swinney, Z.-S. She, Scaling in three-dimensional and quasi-two-dimensional rotating turbulent flows, Phys. Fluids 15 (2003) 2091.

[23] W.-C. Műller, M. Thiele, Scaling and energy transfer in rotating turbulence, Europhys. Lett. 77 (2007) 34003.

[24] J. Seiwert, C. Morize, F. Moisy, On the decrease of intermittency in decaying rotating turbulence, Phys. Fluids 20 (2008) 071702.

[25] M. Thiele, W. C. Muller, Struture and decay of rotating homogeneous turbulence, J. Fluid Mech. 637 (2009) 425–442.

[26] P. Vieillefosse, Local interaction between vorticity and shear in a perfect incompressible fluid, J. Phys. 43 (1982) 837–842.

[27] B. J. Cantwell, Exact solution of a restricted Euler equation for the velocity gradient tensor, Phys. Fluids A 4 (1992) 782–793.

[28] W. T. Ashurst, A. R. Kerstein, R. M. Kerr, C. H. Gibson, Alignment of vorticity and scalar gradient with strain rate in simulated Navier-Stokes turbulence, Phys. Fluids 30 (1987) 2343–2353.

[29] A. Tsinober, E. Kit, T. Dracos, Experimental investigation of the field of velocity-gradients in turbulent flows, J. Fluid Mech. 242 (1992) 169–192.

[30] M. Chertkov, A. Pumir, B. I. Shraiman, Lagrangian tetrad dynamics and the phenomenology of turbulence, Phys. Fluids 11 (1999) 2394–2410.

[31] E. Jeong, S. S. Girimaji, Velocity-gradient dynamics in turbulence: Effect of viscosity and forcing, Theoret. Comput. Fluid Dyn. 16 (2003) 421–432.

[32] A. Naso, A. Pumir, Scale dependence of the coarse-grained velocity derivative tensor structure in turbulence, Phys. Rev. E 72 (2005) 056318.

[33] L. Chevillard, C. Meneveau, Lagrangian dynamics and statistical geometric structure of turbulence, Phys. Rev. Lett. 97 (2006) 174501.

[34] S. Suman, S. S. Girimaji, Homogenized euler equation: a model for compressible velocity gradient dynamics, J. Fluid Mech. 620 (2009) 177–194.

[35] Y. Li, C. Meneveau, Origin of non-Gaussian statistics in hydrodynamic turbulence, Phys. Rev. Lett. 95 (2005) 164502.

[36] Y. Li, C. Meneveau, Intermittency trends and Lagrangian evolution of non-Gaussian statistics in turbulent flow and scalar transport, J. Fluid Mech. 558 (2006) 133–142.

[37] R. H. Kraichnan, Model of intermittency in hydrodynamic turbulence, Phys. Rev. Lett. 65 (1990) 575–578.

[38] K. R. Sreenivasan, R. A. Antonia, The phenomenology of small-scale turbulence, Annu. Rev. Fluid Mech. 29 (1997) 435–472.

[39] Y. Li, L. Chevillard, G. Eyink, C. Meneveau, Matrix exponential-based closures for the turbulent subgrid-scale stress tensor, Phys. Rev. E 79 (2009) 016305.